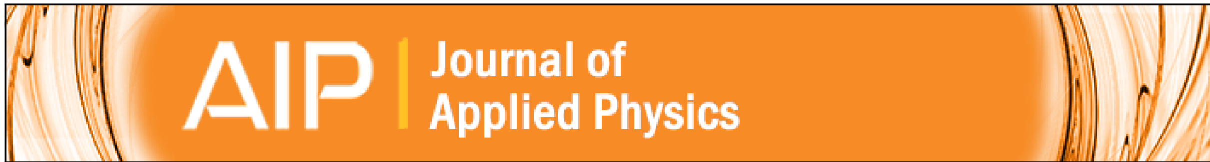

Oxygen species in HfO 2 films: An in situ x-ray photoelectron spectroscopy study

C. Driemeier, R. M. Wallace, and I. J. R. Baumvol

Citation: Journal of Applied Physics **102**, 024112 (2007); doi: 10.1063/1.2759198
View online: http://dx.doi.org/10.1063/1.2759198
View Table of Contents: http://scitation.aip.org/content/aip/journal/jap/102/2?ver=pdfcov
Published by the AIP Publishing

Re-register for Table of Content Alerts

Create a profile.

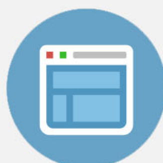

Sign up today!

[This article is copyrighted as indicated in the article. Reuse of AIP content is subject to the terms at: http://scitation.aip.org/termsconditions. Downloaded to] IP: 200.130.19.173 On: Fri, 21 Mar 2014 13:39:04

Oxygen species in HfO_2 films: An *in situ* x-ray photoelectron spectroscopy study

C. Driemeier[a)]
Instituto de Física, Universidade Federal do Rio Grande do Sul, Porto Alegre 91501-970, Brazil and University of Texas at Dallas, Richardson, Texas 75080, USA

R. M. Wallace
Materials Science and Engineering, University of Texas at Dallas, Richardson, Texas 75080, USA

I. J. R. Baumvol
CCET, Universidade de Caxias do Sul, Caxias do Sul 95070-560, Brazil and Instituto de Física, Universidade Federal do Rio Grande do Sul, Porto Alegre 91501-970, Brazil

(Received 30 April 2007; accepted 13 June 2007; published online 25 July 2007)

The chemical bonding of O atoms in HfO_2 films on Si was investigated by *in situ* x-ray photoelectron spectroscopy in the O 1*s* spectral region. In addition to trivial O forming only O-Hf bonds, O 1*s* signals corresponding to nontrivial secondary O (O_{sec}) were also observed. By ruling out possible roles of impurities as well as by comparing O 1*s* signals for different thermochemical processing routes, O_{sec} chemical origins were inferred. Moreover, angle-resolved photoelectron analysis was employed to quantitatively separate surface and bulk O_{sec} contributions. Surface O_{sec} was assigned to surface O-H groups generated either by room temperature water vapor exposure or by 600 °C H_2 annealing. Bulk O_{sec} was assigned to O-O or O-H bonds and, as indicated by thermodynamic calculations and complementary structural analysis, is located in HfO_2 amorphous regions and grain boundaries. This bulk O_{sec} can be partly removed by annealing in reducing atmospheres. For some of the processing routes employed here, we observed additional, water-induced bulk O_{sec}, which was attributed to dissociative water absorption in HfO_2 amorphous regions and O-depleted grain boundaries. © *2007 American Institute of Physics*.
[DOI: 10.1063/1.2759198]

I. INTRODUCTION

Continuous scaling of metal–oxide–semiconductor field-effect transistors (MOSFETs) led traditional SiO_2 and SiO_xN_y gate dielectric films to approach 1 nm thickness in Si-based integrated circuit technologies. Further MOSFET scaling is severely limited by an exponential increase in leakage currents through the gate dielectric due to direct electron tunneling. In order to overcome this limitation, high dielectric constant (high-*k*) materials will replace SiO_2 and SiO_xN_y.[1–3] High-*k* materials allow physically thicker films, which reduce leakage currents, while still increasing MOSFET capacitance density, as required for further MOSFET scaling. HfO_2 emerged as a leading high-*k* candidate due to its high dielectric constant ($k_{HfO_2} \approx 22 \gg k_{SiO_2} = 3.9$),[1,2] thermal stability,[4,5] and sufficient (>1 eV) band offsets to Si.[6,7] However, HfO_2 gate dielectrics usually have high densities of electrically active defects, which degrade MOSFET performance.

Oxygen vacancies and interstitials are the energetically favored intrinsic defects in HfO_2 [8] and first-principles calculations[9–11] provided strong evidence that gap states responsible for trap-assisted tunneling[12] and electron trapping[13] are related to oxygen vacancies in HfO_2. Besides intrinsic defects, extrinsic defects also play an important role. Water vapor present in the atmospheres where HfO_2 films are processed and handled is a ubiquitous potential source of extrinsic hydrogenous defects because water vapor exposures are generally unavoidable in typical MOSFET fabrication facilities. Previous experiments[14] showed that water-derived species can diffuse through HfO_2 at room temperature and may incorporate into HfO_2/Si thin film structures. Moreover, chemical instabilities during annealing of metal/HfO_2 structures were attributed to spurious, water-derived O-H groups present in HfO_2.[15]

In this scenario, identification of all O species in HfO_2 films is a key step in order to understand the origin and nature of O-related intrinsic and extrinsic defects. Due to its sensitivity to all elements (except H) in near surface (up to ~5 nm deep) regions of a sample, as well as its capability to separate different chemical states of an element, x-ray photoelectron spectroscopy (XPS) is a powerful technique to investigate composition and chemical bonding of nanometric films for gate dielectric applications. However, XPS analysis of O signals from oxide films is usually jeopardized by spurious O-containing species that uncontrollably incorporate during film deposition or exposure to air.

We report here on *in situ* sputter deposition, annealing, water vapor exposure, and XPS analysis of nanometric HfO_2 films on Si. All processes were run in an ultrahigh vacuum (UHV) cluster system, without uncontrolled exposures to spurious O species.[16] Analysis of the O 1*s* region of the pho-

[a)]Author to whom correspondence should be addressed; electronic mail: driemeier@if.ufrgs.br; Present address: Instituto de Física, Universidade Federal do Rio Grande do Sul, Av. Bento Gonçalves 9500, Caixa Postal 15051, CEP 91501-970, Porto Alegre, RS, Brazil.

0021-8979/2007/102(2)/024112/8/$23.00 © 2007 American Institute of Physics

[This article is copyrighted as indicated in the article. Reuse of AIP content is subject to the terms at: http://scitation.aip.org/termsconditions. Downloaded to] IP: 200.130.19.173 On: Fri, 21 Mar 2014 13:39:04

TABLE I. Processes applied for the different samples.

Process	UV/O_3 SiO_2	Sputter HfO_2	600 °C 5 min 3×10^{-3} mbar O_2	600 °C 30 min 600 mbar N_2	600 °C 30 min 370 mbar FG	800 °C 30 min 10^{-10} mbar	300 °C 5 min 10^{-10} mbar
as-dep	✓	✓					
O_2 only	✓	✓	✓				✓
O_2+N_2	✓	✓	✓	✓			✓
O_2+FG	✓	✓	✓		✓		✓
O_2+vac	✓	✓	✓			✓	✓

toelectron spectra showed O atoms in HfO_2 which are in addition to trivial O forming only O-Hf bonds. Angle-resolved XPS analysis, variable processing routes, thermodynamic calculations, and complementary structural analysis were employed in order to infer about the nature of the nontrivial O in HfO_2.

II. EXPERIMENTAL DETAILS

P-type Si(100) wafers (100 mm diameter) were cleaned by piranha etch (H_2SO_4/H_2O_2, 3:1) followed by HF strip and Radio Corporation of America cleaning ($NH_4OH/H_2O_2/H_2O$, 1:1:5+$HCl/H_2O_2/H_2O$, 1:1:6). Additional dipping in 2% HF for 1 min followed by 1 min rinsing in 18.1 MΩ de-ionized water was performed immediately before wafer insertion into the UHV cluster system.

The Si wafers were oxidized *in situ* for 60 min using a room temperature ultraviolet/ozone (UV/O_3) process. In this oxidation process UV radiation from a Hg vapor, quartz envelope lamp interacts with O_2 molecules generating O_3 and O^* radicals that oxidize the Si surface, resulting in 1 nm thick, high-quality SiO_2/Si.[17] Oxidation was run with 600 mbar O_2 in the UV/O_3 chamber and the Hg vapor lamp was placed close (~1 cm) to the polished wafer surface. As the next step, HfO_2 was deposited *in situ* by sputtering from a HfO_2 target (99.9%) using 70 sccm, 0.016 mbar Ar as the sputtering gas. The base pressure in the sputtering chamber was $<10^{-8}$ mbar and sputtering power density was 0.5 W/cm^2.

Selected wafers were annealed at 600 °C for 5 min in 3×10^{-3} mbar of O_2 in an attached annealing chamber (base pressure $<10^{-8}$ mbar). Following this first annealing step, selected wafers were further annealed for 30 min at (i) 600 °C in 600 mbar N_2, (ii) 600 °C in 370 mbar forming gas (H_2:N_2, 1:9, hereafter called FG),[18] or (iii) 800 °C in UHV (10^{-10} mbar). All annealed samples presented hydrocarbon contamination that was partly removed by an additional 300 °C, 5 min, UHV (10^{-10} mbar) final anneal, as determined by XPS analysis. The processes applied to the five samples of this study (as-deposited, O_2 only, O_2+N_2, O_2+FG, and O_2+vac) are summarized in Table I.

After the annealing steps, room temperature water vapor exposures were performed in an attached chamber. With the chamber initially in static vacuum ($<10^{-8}$ mbar), a valve to a glass ampule containing liquid water in equilibrium with its vapor is opened for a few seconds, allowing water vapor to enter into the chamber and to interact with the samples. The vapor is pumped away after 15 min of water vapor exposure. The water used in these experiments is 99.9% enriched in the ^{2}H isotope aiming at performing isotopic tracing experiments to be reported elsewhere.

XPS analysis was performed *in situ* (analysis chamber at $<10^{-10}$ mbar), either before or after water vapor exposures, using a monochromatic Al $K\alpha$ ($h\nu$=1486.6 eV) x-ray source and a hemispheric electrostatic electron energy analyzer.[19] Spectra were taken at photoelectron take-off angles of 20°, 45°, and 55° (measured between analyzer axis and sample normal). Before acquiring each spectrum, samples were aligned by maximizing photoelectron count rate. Analyses are run with Si substrates electrically grounded to the electron analyzer and the binding energy scale was calibrated[20] using Au $4f_{7/2}$ (83.96 eV), Ag $3d_{5/2}$ (368.21 eV), and Cu $2p_{3/2}$ (932.62 eV) photoelectron lines.

Grazing-incidence x-ray diffraction (GIXRD) was performed *ex situ* using a Rigaku Ultima III diffractometer with Cu $K\alpha$ x-ray source and 0.5° x-ray incidence angle. In addition, high-resolution transmission electron microscopy (HRTEM) was performed for the O_2 only sample. HfO_2 film thickness of 4.7 nm was measured from the HRTEM cross-section images.

III. RESULTS

A. O 1*s* peak fitting

The O 1*s* region of the photoelectron spectra for the O_2+N_2 sample is shown in Fig. 1, illustrating the general features observed for all samples. The components of the O1*s* spectra were deconvoluted by peak fitting using the XPSPEAK 4.1 code,[21] performing Shirley background subtraction and assuming that each spectrum is composed by two features: the main peak at ~531.8 eV (Ref. 22) and the secondary peak at binding energies 1.4–1.6 eV higher than the main peak. We hereafter refer to O contributing to these peaks as O_{main} and O_{sec}, respectively. Meanwhile, O_{main} can be straightforwardly attributed to trivial O forming only O-Hf bonds in HfO_2,[23–25] the chemical origins of O_{sec} are unknown and are purpose of this work.

By assuming that all nontrivial O contributes to O_{sec} peaks, we do not claim that O_{sec} corresponds to a single chemical species. Possible diversity of contributions to O_{sec} peaks is addressed in the fitting procedure by leaving peak parameters free from fitting constrains, allowing the diversity of contributions to appear, for example, as broader peaks. O_{main} peaks, on the other hand, correspond to O-Hf bonds only, and therefore fitting constraints were applied to this feature. From the four fitting parameters that characterize a

[This article is copyrighted as indicated in the article. Reuse of AIP content is subject to the terms at: http://scitation.aip.org/termsconditions. Downloaded to] IP: 200.130.19.173 On: Fri, 21 Mar 2014 13:39:04

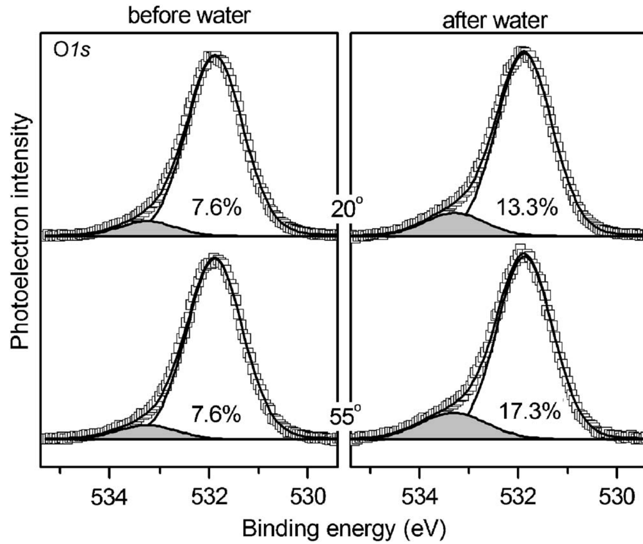

FIG. 1. O 1*s* spectra (symbols) and peak fitting (lines) for the N_2+O_2 sample measured at 20° and 55° take-off angles, either before or after water vapor exposure. Gray-filled peaks correspond to O_{sec} and percentages are O_{sec} relative intensities.

peak, viz., binding energy, intensity (peak area), full width at half maximum (FWHM), and Lorentzian ratio (peaks are a Lorentzian–Gaussian mix), we constrained FWHM and Lorentzian ratio of O_{main} peaks to be unique for a given applied process, independent on photoelectron take-off angles.

The O_{main} intensities before water exposures are the same (within 5%) for the different processing routes, being reduced by 5%–10% after water exposures, which is attributed to water-induced surface layers attenuating O 1*s* signals coming from underlying O_{main}. Nevertheless, in the following angle-resolved XPS analysis the only fitting outputs employed are O_{sec} relative intensities, R, defined as O_{sec}/O_{main} intensity ratios. Uncertainties in R are estimated by varying background subtraction and peak fitting and checking for corresponding variations in R. Error bars shown for R correspond to estimates of $\pm 2\sigma$, accounting for about 95% probability that the actual R lies within the error bars.

B. O 1*s* angle-resolved analysis

The depth distribution of O_{sec} was investigated by analyzing R as a function of photoelectron take-off angle. Assuming that (i) HfO_2 is thick enough to be considered semi-infinite regarding the O 1*s* signals, (ii) O_{sec} and O_{main} are uniformly distributed through HfO_2 with concentrations $[O_{sec}^{bulk}]$ and $[O_{main}^{bulk}]$ (in atoms/cm^3), respectively, and (iii) O_{sec} is also at a surface delta layer with density $[O_{sec}^{surf}]$ (in atoms/cm^2), one derives (see the Appendix)

$$R = \frac{[O_{sec}^{bulk}]}{[O_{main}^{bulk}]} + \frac{[O_{sec}^{surf}]}{[O_{main}^{bulk}]\lambda \cos(\theta)}, \tag{1}$$

where λ is the attenuation length of O 1*s* photoelectrons in HfO_2 and θ is the photoelectron take-off angle. The validity of the assumptions underlying Eq. (1) is discussed in Sec. IV.

By plotting R vs $1/\cos(\theta)$, Eq. (1) corresponds to a straight line in the *y*-intercept/slope mode, where

TABLE II. Conversion factors from linear fitting coefficients to O_{sec} amounts.

Fitting coefficient	O_{sec} location	Coefficient → O_{sec} amount
Intercept	Bulk	$1\% \rightarrow 5.6\times10^{20}$ O_{sec} cm^{-3}
Slope	Surface	$1\% \rightarrow 7.2\times10^{13}$ cm^{-2}

$[O_{sec}^{bulk}]/[O_{main}^{bulk}]$ is the y intercept and $([O_{sec}^{surf}]/[O_{main}^{bulk}])\lambda$ is the slope. Assuming $[O_{main}^{bulk}]$ as the O concentration in stoichiometric bulk HfO_2 with a density 9.8 g/cm^3,[26] one has $[O_{main}^{bulk}]=5.6\times10^{22}$ cm^{-3}. In addition, following procedures developed for calculating λ,[27,28] one derives $\lambda=13$ Å for O 1*s* photoelectrons (kinetic energy ~954 eV) in HfO_2. With these values for $[O_{main}^{bulk}]$ and λ, intercepts and slopes can be proportionally converted to bulk O_{sec} concentrations, $[O_{sec}^{bulk}]$, and surface O_{sec} densities, $[O_{sec}^{surf}]$, respectively. Table II shows the factors that apply for these conversions. Conversion factors accuracies are estimated to be within 20% for intercepts and 30% for slopes.

Figure 2(a) shows O_{sec} relative intensities before water exposures (R_{before}) as a function of $1/\cos(\theta)$ for all the applied processes. The experimental data are fitted with straight lines and derived intercepts and slopes are shown in Figs. 2(b) and 2(c), respectively. Error bars for intercepts and slopes correspond to linear propagation of error bars for R. Additional O_{sec} relative intensities after water exposures ($R_{after}-R_{before}$) as a function of $1/\cos(\theta)$ are shown in Fig. 3(a). Linear fitting to the data was performed, with derived intercepts and slopes shown in Figs. 3(b) and 3(c), respectively. The chemical origins of the observed intercepts and slopes, corresponding to bulk and surface O_{sec}, respectively, are discussed in Sec. IV.

C. Controlling impurities

Within typical XPS detection limits (~1 at. %), C is the only extraneous element present in the samples. The highest C 1*s* intensity [see Fig. 4(a)] corresponds to 2 at. % C. Angle-resolved analysis (not shown) indicates that this C is at surfaces. Nevertheless, the C 1*s* signals observed at ~286 eV correspond to C-H bonds.[29] Signals at ~290 eV, corresponding to C-O bonds, were not observed, indicating

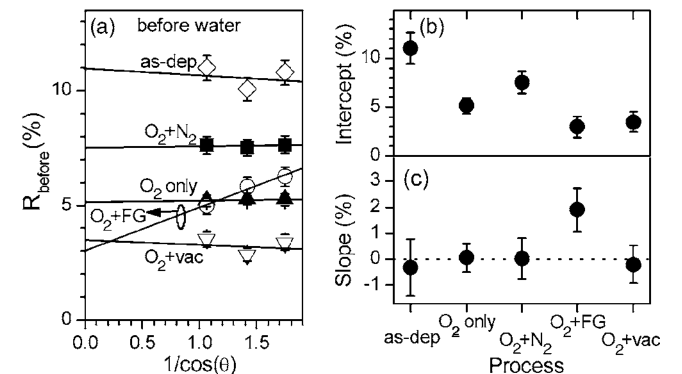

FIG. 2. (a) Linear fitting (solid lines) and experimental (symbols) O_{sec} relative intensities before water vapor exposure (R_{before}) as a function of $1/\cos(\theta)$ for the different applied processes. (b) Intercepts and (c) slopes derived from the linear fitting in (a).

[This article is copyrighted as indicated in the article. Reuse of AIP content is subject to the terms at: http://scitation.aip.org/termsconditions. Downloaded to] IP: 200.130.19.173 On: Fri, 21 Mar 2014 13:39:04

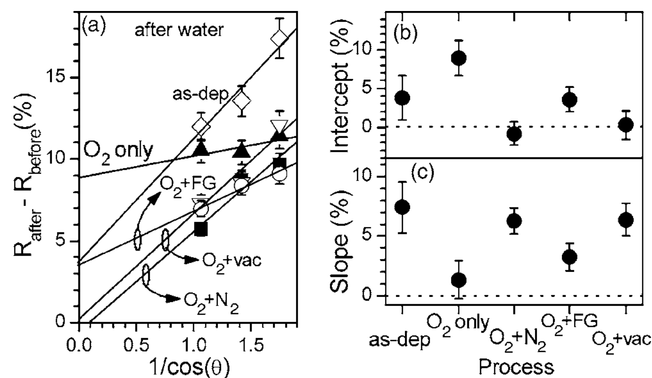

FIG. 3. (a) Linear fitting (solid lines) and experimental differences (symbols) between O_{sec} relative intensities after and before water vapor exposure ($R_{after}-R_{before}$) as a function of $1/\cos(\theta)$ for the different applied processes. (b) Intercepts and (c) slopes derived from the linear fitting in (a).

C-O concentrations below 0.5 at. %. This implies that the several percent O_{sec} relative intensities (Fig. 2) is not consistent with an assignment to C-O bonds. The same conclusion is derived from the C 1*s* spectra taken after water vapor exposures (not shown).

Considering possible contribution of Si-O bonds to the O 1*s* spectra, we first note that, in contrast with previous studies that employed thinner HfO_2 and assigned the secondary O 1*s* peak to interface Si-O bonds,[23,25] the HfO_2 films employed here are thick enough to suppress O 1*s* signals from Si-O bonds in the interface region (see Sec. IV). Moreover, we modeled what would be the contribution to the Si 2*p* spectrum if 1% of the O atoms in HfO_2 would be bonded to spurious Si [see Fig. 4(b)]. For this modeling we used Eq. (A2) (see the Appendix), calculated values for λ,[27–30] and a Si 2*p* peak at binding energies 1.7 eV lower than the SiO_2 peak (corresponding to Si-O diluted in HfO_2).[31] It is clear from the comparison between model and experiment that the Si-O relative concentration in HfO_2 must be below the modeled 1%, implying that the several percent O_{sec} relative intensities (Fig. 2) is not consistent with an assignment to Si-O bonds. Figure 4(b) only shows the Si 2*p* spectrum for the O_2+N_2 sample, but the same conclusion holds for the other samples as well (not shown).

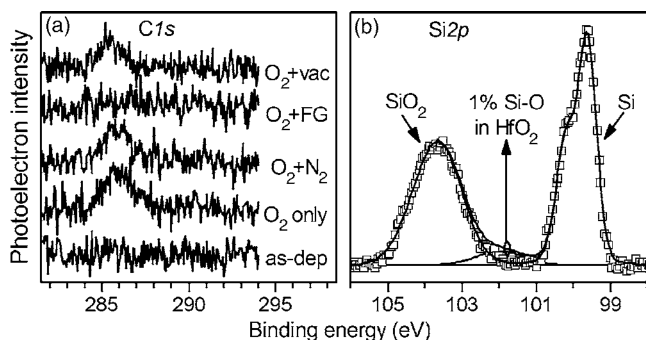

FIG. 4. (a) C 1*s* spectra for the different samples before water exposure. (b) Si 2*p* spectrum (symbols) and peak fitting (lines) for the O_2+N_2 sample. The gray-filled peak is a modeled contribution of 1% (relative O concentration) Si-O bonds in HfO_2. Spectra from (a) and (b) were taken at 20° photoelectron take-off.

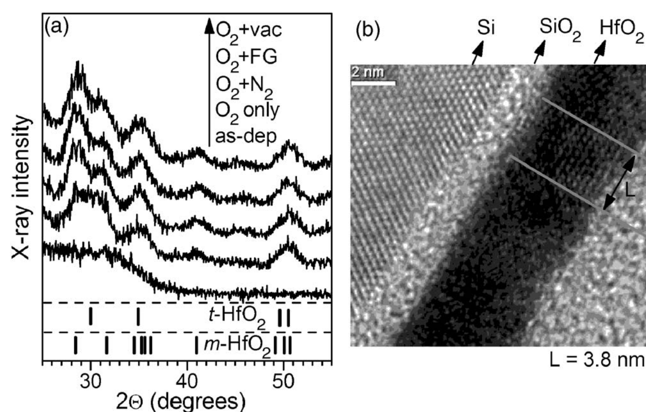

FIG. 5. (a) GIXRD patterns for the different applied processes. Vertical bars correspond to *t*-HfO_2 and *m*-HfO_2 peak positions. (b) HRTEM cross-section image of the O_2-only sample. Characteristic HfO_2 grain dimension (L =3.8 nm) is marked.

From SiO_2 and substrate Si intensity ratios, Si 2*p* spectra also allow determining the thicknesses of interfacial SiO_2 layers (see Ref. 32 for the equation and parameters employed). The SiO_2 thickness is 1.0 nm for the as-deposited (as-dep) sample. It grows to 1.6 nm by annealing in O_2 (O_2 only sample) and it remains constant after subsequent 800 °C annealing in UHV (O_2+vac sample). On the other hand, SiO_2 thicknesses grows to 2.1 nm by additional annealing in N_2 or FG (O_2+N_2 and O_2+FG samples), indicating presence of oxidizing residuals in these annealing atmospheres. Room temperature water vapor exposures did not promote measurable (>0.2 nm) SiO_2 growth in any sample.

D. Structural analysis

Figure 5(a) shows GIXRD patterns for all the samples of this study. While for the as-dep sample the pattern is smooth, indicating fully amorphous HfO_2, for the annealed samples there are diffraction peaks, identified with monoclinic (*m*-HfO_2) and tetragonal (*t*-HfO_2) phases. Among the annealed samples, those submitted to a second high temperature anneal (O_2+N_2, O_2+FG, and O_2+vac) have diffraction patterns indistinguishable from one another, but which differ (especially for $28° < 2\Theta < 32°$) from the pattern for the O_2 only sample. This difference is attributed to incomplete HfO_2 crystallization (indicating remaining amorphous HfO_2) for the sample only annealed in O_2, while further high temperature annealing completes crystallization. This behavior agrees with the observed onset for HfO_2 crystallization at ~600 °C.[25,33]

Figure 5(b) shows the HRTEM cross-section image of the O_2 only sample, indicating the presence of HfO_2 and SiO_2 layers as well as the crystalline Si substrate. The electron beam, which was aligned with the Si [100] direction, also appears to have been incidentally aligned with an axis or plane of a HfO_2 crystallite. When this happens, one may observe a single HfO_2 crystallite and determine an approximate grain dimension parallel to the interfaces, L, as shown in Fig. 5(b). An average L of 6.0 nm with standard deviation of 2.5 nm was determined from HRTEM images taken at different spots.

[This article is copyrighted as indicated in the article. Reuse of AIP content is subject to the terms at: http://scitation.aip.org/termsconditions. Downloaded to] IP: 200.130.19.173 On: Fri, 21 Mar 2014 13:39:04

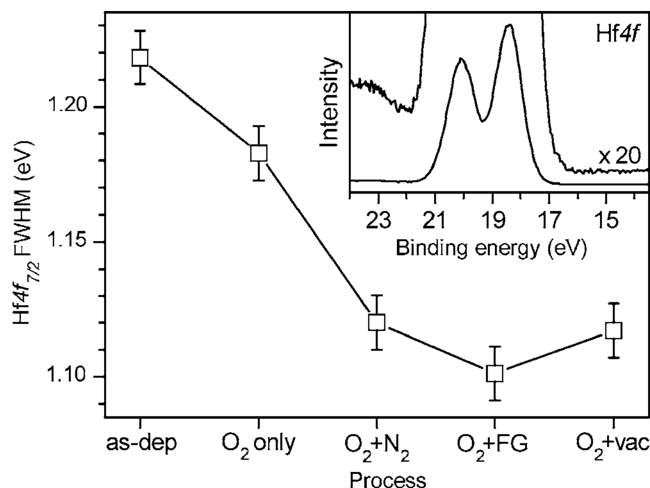

FIG. 6. Hf $4f_{7/2}$ FWHM for the different applied processes and Hf $4f$ spectrum for the O_2+N_2 sample (inset). Measurements were performed before water vapor exposures, at 20° photoelectron take-off.

E. Hf 4*f* features

The inset of Fig. 6 shows the Hf $4f$ spectrum for the O_2+N_2 sample, illustrating the features observed for all the samples. One observes a single Hf component, corresponding to O-Hf bonds, with the 1.65 eV spin-orbit splitting between Hf $4f_{7/2}$ and Hf $4f_{5/2}$ photoelectrons. The same spectrum with intensity multiplied by 20 evidences no additional Hf $4f$ features. Figure 6 also shows the Hf $4f_{7/2}$ FWHM (as derived from peak fitting) for the different applied processes. The observed higher Hf $4f_{7/2}$ FWHM for the as-dep and O_2 only samples are attributed to amorphous HfO_2 present in these samples, as detected by GIXRD. Correspondingly higher FWHM for O_{main} peaks (in the O 1s spectra) could not be established due to worse O_{main} peak width precision.

IV. DISCUSSION

A. Validity of the angle-resolved model

The validity of the assumptions underlying the angle-resolved model for O_{sec} relative intensities is discussed later.

(i) HfO_2 is semi-infinite regarding O 1s signals – This assumption is supported by the absence of significant O 1s signal coming from the interfacial SiO_2 layers. Since O in SiO_2 leads to O 1s peaks at binding energies close to those observed for O_{sec},[23,25,31] if the underlying SiO_2 contributed to the O 1s spectra, then one should observe a component of R approximately proportional to the attenuation due to the HfO_2 overlayer, $R \sim \exp[-t/\lambda \cos(\theta)]$, where t is the HfO_2 thickness and $t/\lambda \sim 3$. Judging from the data in Fig. 2(a), any contribution to R with such behavior is negligibly small.

(ii) Bulk O_{sec} and O_{main} concentrations are independent with depth – First, deposition conditions and thermal budgets are constant through the HfO_2 films examined, which is a necessary condition to assume that film chemistries do not depend on depth. Moreover, we observed R_{before} independent on take-off angle [Fig. 2(a), the exception for the O_2+FG sample is explained later], which would not be observed if O chemistries depended on depth.

(iii) Surface O_{sec} densities can be approximated by surface delta layers – An O_{sec} surface delta layer means that (a) O_{sec} is at the surface and (b) the O_{sec} surface layer does not attenuate signals from O underneath. Support for (a) comes entirely from specificity of surface chemistries because angle-resolved XPS alone, due to intrinsic depth resolution limits,[34] would not distinguish possible near-surface (up to a few angstroms deep) O_{sec} contributions. Regarding (b), neglected surface attenuation overestimates surface O_{sec} densities by 5%–10% (typical water-induced surface attenuation observed for O_{main} intensities). Bulk O_{sec} concentrations, on the other hand, are correctly estimated by the employed model because the neglected surface attenuation is identical for photoelectrons originating from bulk O_{sec} and from bulk O_{main} reference.

B. Surface O_{sec}

Water-induced surface hydroxylation is a common phenomenon in transition metal oxides,[35] is well established for atomic layer deposition techniques that use water as a HfO_2 deposition precursor,[36] and was observed by exposing HfO_2 films to water vapor at room temperature, leading to an O 1s peak at binding energies close to those of O_{sec}.[14] Based on these facts, we assign the additional surface O_{sec} due to water exposure [Fig. 3(c)] to surface hydroxylation. It was proposed[14,35,37,38] that a H_2O molecule decomposes by attaching an O-H group to surface Hf and the remaining H to a neighbor surface O, forming two hydroxyls for each dissociatively adsorbed water molecule. This reaction was calculated to be exothermic by 90–180 kJ mol^{-1} at the m-HfO_2(001) surface[37,38] and by 60–86 kJ mol^{-1} at the m-$HfO_2(\underline{1}11)$ surface.[38]

Besides surface O_{sec} due to water, there is an O_{sec} surface density of $1.4\pm0.6\times10^{14}$ cm^{-2} [from Fig. 2(c) and Table II] for the O_2+FG sample before water exposure. This surface O_{sec} is attributed to O-H groups created by reaction of the HfO_2 film surface with H_2 from the 600 °C FG annealing. This is in reasonable agreement with $2.2\pm0.1\times10^{14}$ ^{2}H cm^{-2} observed to incorporate at HfO_2 surfaces by annealing in $^2H_2$ (600 °C, 30 min),[39] as well as in qualitative agreement with O-H groups that form at ZrO_2 (chemically similar to HfO_2) surfaces by annealing in H_2.[40] Moreover, dissociative H_2 adsorption (forming O-H and Zr-H bonds) was calculated[41] to be exothermic by 17.8 kJ mol^{-1} at the t-ZrO_2 (101) surface.

C. Bulk O_{sec} – Location

We describe the HfO_2 films as consisting of ordered regions, corresponding to HfO_2 within crystallites (with or without point defects), and disordered regions, corresponding to HfO_2 amorphous regions, grain boundaries, surfaces, and interfaces. First of all, bulk O_{sec} cannot be assigned to

[This article is copyrighted as indicated in the article. Reuse of AIP content is subject to the terms at: http://scitation.aip.org/termsconditions. Downloaded to] IP: 200.130.19.173 On: Fri, 21 Mar 2014 13:39:04

defect-free crystallites because O atoms in ideal t-HfO_2 and m-HfO_2 are all derived from equivalent O atoms in c-HfO_2 and would not lead to an O_{sec} peak shifted from O_{main} peak by considerable 1.4–1.6 eV.

Moreover, considering the presence of O vacancies and interstitials within HfO_2 crystallites, the equilibrium relative concentration of the point defects can be approximated by $\exp(-E\pm\mu_O/k_BT)$, where E is the formation energy of the defect (referenced to half the energy of an isolated O_2 molecule), μ_O is the chemical potential for O atoms, k_B is the Boltzmann constant, and T is the temperature in Kelvin. The "+" holds for interstitials and the "–" for vacancies. Such a simple thermodynamic model assumes that the presence of the intrinsic defects is not controlled by reaction kinetics, which is supported by fast O diffusion observed in HfO_2.[42,43] First-principles calculations determined $E=1.6$ eV for O interstitials[8] and $E=6.4$ eV for O vacancies.[8,44] Moreover, considering μ_O to be that of an ideal O_2 gas,

$$\mu_O=\frac{1}{2}k_BT\ln\left[\frac{P}{k_BT}\left(\frac{2\pi\hbar^2}{m_{O_2}k_BT}\right)^{3/2}\right],$$

and calculating μ_O for a pressure (P) of 10^{-3} mbar of O_2 and $T=873$ K (600 °C), which is a typical experimental condition employed here, one obtains $\mu_O=-2.1$ eV. Applying μ_O and E to the exponential factor leads to relative defects concentrations of $\sim 10^{-22}$ for O interstitials and $\sim 10^{-25}$ for O vacancies. Performing similar calculation for H interstitial in HfO_2 [using $E=2.0$ eV (Ref. 45) and $P_{H_2}=10^{-8}$ mbar], one derives relative H concentration of $\sim 10^{-25}$. Since all considered defects are expected in relative concentrations far lower than the few percent relative concentrations observed for bulk O_{sec}, it is very likely that bulk O_{sec} is not within HfO_2 crystallites. Instead, bulk O_{sec} is in disordered HfO_2, i.e., in amorphous regions and grain boundaries.

Considering a polycrystalline oxide, the ratio between O concentration at grain boundaries and inside crystallites can be approximated by

$$\frac{[O_{boundary}]}{[O_{inside}]}\sim\frac{\sigma A}{\rho V},$$

where σ is the density of O atoms at a HfO_2 surface, ρ is the concentration of O atoms in HfO_2, A is a typical grain area, and V is a typical grain volume. Assuming $\sigma\sim\rho^{2/3}$ and $A/V\sim 1/L$, where L is a typical grain dimension parallel to the interfaces, and using $\rho=5.6\times10^{22}$ O cm^{-2} (as previously used for $[O^{bulk}_{main}]$) and $L=6.0$ nm (average L from HRTEM images), one obtains $[O_{boundary}]/[O_{inside}]\sim 4\%$. This percentage is in good agreement with observed bulk O_{sec}/O_{main} ratios before water vapor exposure [Fig. 2(b)], further supporting O_{sec} location in disordered regions such as grain boundaries. In the case of the as-dep HfO_2, which is amorphous (fully disordered according to our description), most O still contributes to the O_{main} peak, implying that in disordered regions not all O atoms correspond to O_{sec}, but rather that O_{sec} and O_{main} coexist.

D. Bulk O_{sec} – Removal by FG annealing

It is worth comparing the O_2+N_2 and O_2+FG samples, both with fully crystallized HfO_2, because they were exposed to identical thermal budgets and, therefore, should have very similar distribution of crystallites and grain boundaries. Nevertheless, one observes lower bulk O_{sec} concentration for the O_2+FG sample [Fig. 2(b)], indicating that bulk O_{sec} from grain boundaries was party removed by the reducing FG annealing. Such O_{sec} removal might leave O-vacancy-like defects at HfO_2 grain boundaries.

E. Bulk O_{sec} – Chemical nature

Having ruled out the presence of impurities (except H), we restrict the discussion of bulk O_{sec} bonding to three chemical elements: Hf, O, and H.

(i) Modified O-Hf bonds (bonds with nontrivial length and/or formed between atoms with nontrivial coordination numbers) are expected in HfO_2 disordered regions.[46] Nevertheless, judging from surface disorder that does not lead to surface O_{sec} [Fig. 2(c)], and from the Hf 4f spectra, where disorder appears as broader, but not as separated peaks (Fig. 6), it is unlikely that bulk O_{sec} corresponds to modified O-Hf bonds.

(ii) O-O bonds lead to less negative net charges at O atoms, which typically imply higher binding energies for the corresponding O 1s photoelectrons. Such qualitative binding energy difference was observed between O_{sec} and O_{main} peaks, indicating that bulk O_{sec} possibly corresponds to O-O bonds.

(iii) O-H bonds might be formed during HfO_2 deposition by reaction of O dangling bonds with H_2 molecules. Such reaction was observed in SiO_2 (Ref. 47) and the concentration of H_2 residuals in the deposition atmospheres is enough to explain O_{sec} relative concentrations.[48] Moreover, binding energies of O_{sec} peaks are fully compatible with O-H bonds (e.g., surface O_{sec} assigned to O-H). Judging from the earlier-mentioned facts, it is likely that bulk O_{sec} observed before water exposure corresponds to O-H bonds.

Now consider the additional bulk O_{sec} that appears after water exposures [Fig. 3(b)]. Ruling out nondissociative water absorption because it typically leads to O 1s photoelectrons at binding energies 1.0–1.5 eV higher than those observed for O_{sec},[35,49] we attribute water-induced bulk O_{sec} to dissociative water absorption (hydroxylation). Water-induced bulk O_{sec} was observed for the samples with HfO_2 amorphous regions (as-dep and O_2 only), whereas it was not observed for the O_2+N_2 and O_2+vac samples with fully crystallized HfO_2 [Fig. 3(b)]. A previous study[15] observed water-induced bulk O-H groups in a HfO_2 film grown at low temperature (presumably amorphous), whereas not detecting such signal for HfO_2 grown at higher temperature (presumably crystallized). Another study[14] failed to detect water absorption into 800 °C-vacuum-annealed, fully crystallized HfO_2 films. These previous results, as well as the results presented here, suggest that amorphous HfO_2 absorbs water, whereas polycrystalline HfO_2 does not.

[This article is copyrighted as indicated in the article. Reuse of AIP content is subject to the terms at: http://scitation.aip.org/termsconditions. Downloaded to] IP: 200.130.19.173 On: Fri, 21 Mar 2014 13:39:04

However, the O_2+FG sample is an exception to this rule. In this case, the HfO_2 film is fully crystallized and water-induced bulk O_{sec} [Fig. 3(b)] is attributed to hydroxylation of grain boundaries from where bulk O_{sec} had been removed by the FG annealing. In general, we suggest that hydroxylation of HfO_2 amorphous regions and O-depleted grain boundaries relies on the presence of atomic-scale voids, which allow net incorporation of water-derived atoms while avoiding energy-costly displacements of neighbor HfO_2. Finally, typical MOSFET processing includes a $\sim$1000 °C activation annealing that might desorb the O_{sec}-related species from HfO_2, possibly leading to deleterious chemical reactions with the overlying gate electrode.[15]

V. CONCLUSIONS

In summary, we performed *in situ* sputter deposition, annealing, room temperature water vapor exposure, and XPS analysis of HfO_2 nanometric films on Si. Each O 1*s* photoelectron spectrum was deconvoluted into two O peaks: one main peak, corresponding to trivial O forming O-Hf bonds, and one secondary peak, corresponding to nontrivial secondary O (O_{sec}) whose origins were investigated here.

Besides ruling out possible roles of impurities (except H) on O_{sec} bonding, an angle-resolved XPS model was employed in order to quantitatively separate HfO_2 surface and bulk contributions to O_{sec}. Surface O_{sec} was attributed to HfO_2 surface hydroxyls induced either by room temperature water vapor exposure or by 600 °C H_2 annealing. HfO_2 surface hydroxylation might become significant for metal/HfO_2 interface engineering in HfO_2-based MOSFETs.

Bulk O_{sec} was attributed primarily to O-H bonds and, as indicated by thermodynamic calculations and structural analyses, is located in HfO_2 amorphous regions and grain boundaries. Moreover, this bulk O_{sec} could be partly removed by annealing in reducing, H_2-containing atmospheres, which might leave O-vacancy-like defects. For HfO_2 films with amorphous regions or O-depleted grain boundaries we also observed additional, water-induced bulk O_{sec} attributed to HfO_2 bulk hydroxylation. Finally, the presence of nontrivial O, either induced by water or not, indicates that HfO_2 amorphous regions and grain boundaries might contain O-related defects without counterparts within HfO_2 crystallites.

ACKNOWLEDGMENTS

The authors acknowledge the CAPES-UTD Cooperation Agreement for financial support. The authors also acknowledge Professor M. J. Kim, F. S. Aguirre-Testado, P. Sivasubramani, C. Floresca, D. Dha, and B. Kim for their assistance on conducting this work.

APPENDIX

The intensity of an XPS signal (peak area) for a given chemical state X of a given element core level can be expressed as[34]

$$I_X(\theta) = FT_XA_X\sigma_XL_X\int_0^\infty C_X(z)\exp\left[\frac{-z}{\lambda_X(z)\cos(\theta)}\right]dz, \quad \text{(A1)}$$

where F is the x-ray photon flux, T_X is the transmission function of the electron analyzer, A_X is the analysis area, σ_X is the cross section of the photoemission process, L_X is the asymmetry factor, $C_X(z)$ is the concentration of atoms in the chemical state X as a function of depth z (z=0 at the surface), $\lambda_X(z)$ is the attenuation length, and θ is the photoelectron take-off angle. All terms labeled with an X subscript depend on the core level under analysis. If one is interested only in the ratio R between the intensities of two chemical states X and Y of the same core level, $R(\theta)=I_X(\theta)/I_Y(\theta)$, then F, T, A, σ, and L cancel, since they are identical for X and Y. Moreover, if we further assume a homogenous media, then λ has a single value for X and Y, independent on z, and $R(\theta)$ can be expressed as

$$R(\theta) = \frac{\int_0^\infty C_X(z)\exp\left[\frac{-z}{\lambda\cos(\theta)}\right]dz}{\int_0^\infty C_Y(z)\exp\left[\frac{-z}{\lambda\cos(\theta)}\right]dz}. \quad \text{(A2)}$$

If $C(z)=C$, independent on z, then the integrals simplify to

$$\int_0^\infty C\exp\left[\frac{-z}{\lambda\cos(\theta)}\right]dz = C\lambda\cos(\theta). \quad \text{(A3)}$$

Moreover, if $C(z)$ is a surface delta layer, $C(z)=D\delta(z-\varepsilon)$, where D is a surface atomic density (in atoms/cm^2), δ is the delta function, and ε is a positive infinitesimal quantity introduced to mathematically remove the delta peak from the lower integration limit, then the integral simplifies to

$$\lim_{\varepsilon\to 0^+}\int_0^\infty D\delta(z-\varepsilon)\exp\left[\frac{-z}{\lambda\cos(\theta)}\right]dz = D. \quad \text{(A4)}$$

Now consider that

$$C_X(z) = C_X + D_X\delta(z-\varepsilon), \quad \text{(A5a)}$$

$$C_Y(z) = C_Y. \quad \text{(A5b)}$$

By substituting $C_X(z)$ and $C_Y(z)$ from Eqs. (A5a) and (A5b) into Eq. (A2) and solving the integrals according to Eqs. (A3) and (A4), we obtain

$$R(\theta) = \frac{C_X\lambda\cos(\theta)+D_X}{C_Y\lambda\cos(\theta)} = \frac{C_X}{C_Y} + \frac{D_X}{C_Y\lambda\cos(\theta)}. \quad \text{(A6)}$$

Labeling C_X, D_X, and C_Y as $[O_{sec}^{bulk}]$, $[O_{sec}^{surf}]$, and $[O_{main}^{bulk}]$, respectively, leads us to the expression of Eq. (1). The term between the equal signs in Eq. (A6) allows simple interpretation of the formula: R is the ratio between effective densities (in atoms/cm^2) contributing to the XPS signal. Surface atoms contribute integrally, with a density D, while bulk atoms contribute up to an effective depth $\lambda\cos(\theta)$, with a density $C\lambda\cos(\theta)$.

[1]J. Robertson, Rep. Prog. Phys. **69**, 327 (2006).

[This article is copyrighted as indicated in the article. Reuse of AIP content is subject to the terms at: http://scitation.aip.org/termsconditions. Downloaded to] IP: 200.130.19.173 On: Fri, 21 Mar 2014 13:39:04

[2] *High-k Gate Dielectrics*, edited by M. Houssa (Institute of Physics, Bristol, 2004).

[3] G. D. Wilk, R. M. Wallace, and J. M. Anthony, J. Appl. Phys. **89**, 5243 (2001).

[4] K. J. Hubbard and D. G. Schlom, J. Mater. Res. **11**, 2757 (1996).

[5] M. Gutowski, J. E. Jaffe, C. L. Liu, M. Stoker, R. I. Hegde, R. S. Rai, and P. J. Tobin, Appl. Phys. Lett. **80**, 1897 (2002).

[6] J. Robertson, J. Vac. Sci. Technol. B **18**, 1785 (2000).

[7] V. V. Afanas'ev, A. Stesmans, F. Chen, X. Shi, and S. A. Campbell, Appl. Phys. Lett. **81**, 1053 (2002).

[8] A. S. Foster, F. L. Gejo, A. L. Shluger, and R. M. Nieminen, Phys. Rev. B **65**, 174117 (2002).

[9] K. Xiong, J. Robertson, M. C. Gibson, and S. J. Clark, Appl. Phys. Lett. **87**, 183505 (2005).

[10] J. L. Gavartin, D. M. Ramo, A. L. Shluger, G. Bersuker, and B. H. Lee, Appl. Phys. Lett. **89**, 082908 (2006).

[11] P. Broqvist and A. Pasquarello, Appl. Phys. Lett. **89**, 262904 (2006).

[12] M. Houssa, M. Tuominen, M. Naili, V. Afanas'ev, A. Stesmans, S. Haukka, and M. M. Heyns, J. Appl. Phys. **87**, 8615 (2000).

[13] A. Kerber, E. Cartier, L. Pantisano, R. Degraeve, T. Kauerauf, Y. Kim, A. Hou, G. Groeseneken, H. E. Maes, and U. Schwalke, IEEE Electron Device Lett. **24**, 87 (2003).

[14] C. Driemeier, E. P. Gusev, and I. J. R. Baumvol, Appl. Phys. Lett. **88**, 201901 (2006).

[15] M. Copel, R. P. Pezzi, D. Neumayer, and P. Jamison, Appl. Phys. Lett. **88**, 072914 (2006).

[16] F. S. Aguirre-Tostado, D. Layton, A. Herrera-Gomez, R. M. Wallace, J. Zhu, G. Larrieu, E. Maldonado, W. P. Kirk, and M. Tao, J. Appl. Phys. (in press).

[17] G. D. Wilk and B. Brar, IEEE Electron Device Lett. **20**, 132 (1999).

[18] The pressure of the FG annealing atmosphere (370 mbar) was calculated based on 600 mbar reading (identical to N_2 annealing) in a thermal conductivity pressure gauge. Because both pressure and temperature readings depend on the thermal conductivities of the annealing atmospheres, identical pressure reading assures that N_2 and FG annealing are run at identical temperatures.

[19] P. Ruffieux, P. Schwaller, O. Gröning, L. Schlapbach, P. Gröning, Q. C. Herd, D. Funnemann, and J. Westermann, Rev. Sci. Instrum. **71**, 3634 (2000).

[20] See ASTM Standard E-2108–05, www.astm.org.

[21] Avai1able for download at http://www.uksaf.org.

[22] Comparison with published spectra (see Refs. 23–25) suggests that binding energies are shifted by $\sim$0.5 eV due to x-ray-induced positive charges in the SiO_2 interfacial layer.

[23] P. D. Kirsch, C. S. Kang, J. Lozano, J. C. Lee, and J. G. Ekerdt, J. Appl. Phys. **91**, 4353 (2002).

[24] K. Kobayashi *et al.*, Appl. Phys. Lett. **83**, 1005 (2003).

[25] A. Deshpande, R. Inman, G. Jursich, and C. G. Takoudis, J. Appl. Phys. **99**, 094102 (2006).

[26] *CRC Handbook of Chemistry and Physics*, edited by R. C. Weast, M. J. Astle, and W. H. Beyer, 66th ed. (CRC Press, Boca Raton, 1985).

[27] S. Tanuma, C. J. Powell, and D. R. Penn, Surf. Interface Anal. **21**, 165 (1994).

[28] C. J. Powell and A. Jablonski, *NIST Electron Effective-Attenuation-Length Database—Version 1.1* (National Institute of Standards and Technology, Gaithersburg, MD, 2003).

[29] C. D. Wagner, W. M. Riggs, L. E. Davis, J. F. Moulder, and G. E. Muilenberg, *Handbook of X-Ray Photoelectron Spectroscopy* (Perkin-Elmer, Eden Prairie, MN, 1979).

[30] For Si 2p photoelectrons we calculated λ=17.5 Å in HfO_2 and λ=35.9 Å in SiO_2.

[31] G. B. Rayner, D. Kang, Y. Zhang, and G. Lucovsky, J. Vac. Sci. Technol. B **20**, 1748 (2002).

[32] Z. H. Lu, J. P. McCaffrey, B. Brar, G. D. Wilk, R. M. Wallace, L. C. Feldman, and S. P. Tay, Appl. Phys. Lett. **71**, 2764 (1997).

[33] D. A. Neumayer and E. Cartier, J. Appl. Phys. **90**, 1801 (2001).

[34] P. J. Cumpson, J. Electron Spectrosc. Relat. Phenom. **73**, 25 (1995).

[35] M. A. Henderson, Surf. Sci. Rep. **46**, 5 (2002).

[36] M. Ritala, in *High-k Gate Dielectrics*, edited by M. Houssa (Institute of Physics, Bristol, 2004), Chap. 2.1, pp. 17–64.

[37] I. M. Iskandarova, A. A. Knizhnik, E. A. Rykova, A. A. Bagatur'yants, B. V. Potapkin, and A. A. Korkin, Microelectron. Eng. **69**, 587 (2003).

[38] A. B. Mukhopadhyay, J. F. Sanz, and C. B. Musgrave, Chem. Mater. **18**, 3397 (2006).

[39] C. Driemeier, L. Miotti, I. J. R. Baumvol, C. Radtke, E. P. Gusev, M. J. Kim, and R. M. Wallace, Appl. Phys. Lett. **88**, 041918 (2006).

[40] A. Trunschke, D. L. Hoang, and H. Lieske, J. Chem. Soc., Faraday Trans. **91**, 4441 (1995).

[41] A. Hofmann, S. J. Clark, M. Oppel, and I. Hahndorf, Phys. Chem. Chem. Phys. **4**, 3500 (2002).

[42] B. W. Busch, W. H. Schulte, E. Garfunkel, T. Gustafsson, W. Qi, R. Nieh, and J. Lee, Phys. Rev. B **62**, R13290 (2000).

[43] R. M. C. de Almeida and I. J. R. Baumvol, Surf. Sci. Rep. **49**, 1 (2003).

[44] W. L. Scopel, A. J. R. da Silva, W. Orellana, and A. Fazzio, Appl. Phys. Lett. **84**, 1492 (2004).

[45] J. Kang, E. C. Lee, K. J. Chang, and Y. G. Jin, Appl. Phys. Lett. **84**, 3894 (2004).

[46] D. Ceresoli and D. Vanderbilt, Phys. Rev. B **74**, 125108 (2006).

[47] D. L. Griscom, J. Appl. Phys. **58**, 2524 (1985).

[48] A time-integrated flux of $\sim 10^{16}$ H^2 cm^{-2}, which is comparable to $\sim 2.5 \times 10^{16}$ O cm^{-2} present in the HfO_2 films, was calculated using kinetic gas theory and considering H_2 as an important component of the 10^{-8} mbar base pressure of HfO_2 deposition processes.

[49] D. Barreca, G. A. Battiston, R. Gerbasi, and E. Tondello, Surf. Sci. Spectra **7**, 303 (2000).

[This article is copyrighted as indicated in the article. Reuse of AIP content is subject to the terms at: http://scitation.aip.org/termsconditions. Downloaded to] IP: 200.130.19.173 On: Fri, 21 Mar 2014 13:39:04